Atomic and electronic structures of doped silicon nanowires: A first-principles study

E. Durgun,[1,2] N. Akman,[3] C. Ataca,[1,4] and S. Ciraci[1,2,*]
[1]*Department of Physics, Bilkent University, Ankara 06800, Turkey*
[2]*UNAM-Institute for Materials Science and Nanotechnology, Bilkent University, Ankara 06800, Turkey*
[3]*Department of Physics, Mersin University, Mersin 33343, Turkey*
[4]*Department of Electrical and Electronic Engineering, Bilkent University, Ankara 06800, Turkey*
(Received 17 August 2007; revised manuscript received 6 November 2007; published 20 December 2007)

We have investigated the atomic and electronic structures of hydrogen saturated silicon nanowires doped with impurity atoms (such as Al, Ga, C, Si, Ge, N, P, As, Te, Pt) using a first-principles plane wave method. We considered adsorption and substitution of impurity atoms at the surface and also their substitution at the core of the nanowire. In the case of adsorption to the surface, we determined the most energetic adsorption geometry among various possible adsorption sites. All impurities studied lead to nonmagnetic ground state with a significant binding energy. Impurity bands formed at high impurity concentration are metallic for group IIIA and VA elements but are semiconductor and modify the band gap for group IVA and VIA elements. While low substitutional impurity concentration leads to usual *n*- and *p*-type behaviors reminiscent of bulk Si, this behavior is absent if the impurity atom is adsorbed on the surface. It is shown that the electronic properties of silicon nanowires can be modified by doping for optoelectronic applications.

DOI: 10.1103/PhysRevB.76.245323 PACS number(s): 73.63.Nm, 73.20.At, 73.20.Hb

I. INTRODUCTION

Well-developed microelectronic technology based on Si has made silicon nanowires (SiNWs) an attractive material for nanoscale optoelectronics. SiNW can transport charge carriers so efficiently that it can serve as a building material in many electronic and optical applications such as field effect transistors[1] (FETs), light emitting diodes,[2] lasers,[3] and interconnects. Additionally, the conductance of silicon nanowire can be tuned easily by *doping* during the growth process or by applying a gate voltage in a SiNW FET. Up to now, various experimental methods have been used to synthesize the silicon nanowires with different diameters and orientations. Recently, it has become possible to fabricate the thinnest SiNW with a diameter of 1.3–7 nm and their oxide etched surfaces could be terminated with hydrogen.[4] It has also been found that hydrogen passivated SiNW (H-SiNW) is stable and oxidation resistant in air.

Recently, electronic structure and energetics of bare (unpassivated) and surface passivated SiNWs have been treated theoretically. Rurali and Lorente[5] studied bare and undoped SiNWs of various diameters by using density functional theory (DFT). They obtained conducting SiNWs, which result from the energetically equivalent surface reconstructions. The surface reconstruction has also been examined in recent papers.[6,7] Structures and energetics of H-SiNWs were reported by using DFT tight binding method.[8] By passivating the SiNWs surface with H and some halogens including Br, Cl, and I, the electronic structure of wires with diameter ranging from 0.6 to 3 nm has been studied using *ab initio* DFT calculations.[9]

Impurity doped SiNWs have also attracted attention since the dopant atoms provide excess carriers required in device applications, such as diodes and transistors. Doping of H-SiNW by B and P impurities and its effect on the electronic structure and band gap have been investigated by calculations based on DFT.[10] Fernandez-Serra *et al.*[11] examined the transport properties of the B and P doped silicon nanowires. Furthermore, growing research interest has been devoted to the functionalization of SiNW surface with various species to study the chemical and biological sensitivities of silicon nanowires.[12–14] Earlier, we have studied functionalization (and also doping) of SiNWs with specific transition metal (TM) atoms resulting in many interesting nanostructures, such as half-metals, one-dimensional ferromagnetic semiconductor or nanomagnets.[15]

Instead of providing just excess carriers which are necessary for device operation, single dopants in a SiNW can also be used as a functional part of a device. In order to clarify this issue, electronic states of single dopants in gated SiNW (Ref. 16) have been discussed recently. Moreover, variation in electronic properties of silicon clathrate nanowires intercalated with alkaline and alkaline earth atoms has been presented by using a first-principles study.[17]

The present paper reports an extensive analysis of the electronic structure of H-SiNWs doped by various (impurity) adatoms, such as Al, Ga, C, Si, Ge, N, P, As, Te, and Pt. We first examined the adsorption geometry and energetics of these adatoms and their effects on the electronic properties for different concentrations. We also investigated the electronic properties of H-SiNW substitutionally doped by Al or As atoms. We found that the electronic properties of a semiconducting H-SiNW is dramatically altered upon adsorption of adatoms at high concentration. While specific atoms, such as Al, Ga, N, P, and As, metallize H-SiNW, adatoms such as C, Si, Ge, Te, and Pt modify the band gap. Low substitutional impurity concentration results in usual *n*- and *p*-type behaviors.

II. METHOD

We have performed first-principles plane wave calculations[18,19] within DFT (Ref. 20) using ultrasoft pseudopotentials.[19,21,22] The exchange correlation potential

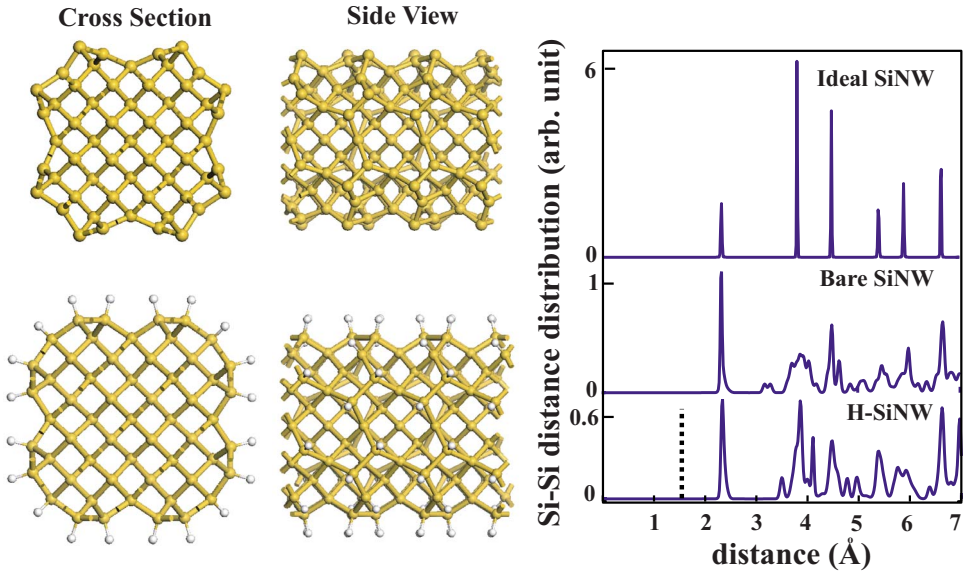

FIG. 1. (Color online) Cross section and side views of optimized bare SiNW (uppermost two panels) and hydrogen passivated SiNW (lower two panels). Side views of the figures are given in three unit cells for clarity. On the right panels, the Si-Si distance distribution up to the sixth nearest neighbors is indicated for ideal SiNW, as cut from bulk crystal, optimized bare SiNW, and hydrogenated SiNW. The dotted line in the third panel represents the H–Si bond population.

has been approximated by generalized gradient approximation (GGA) using PW91 functional[23] both for spin-polarized and spin-unpolarized cases. For partial occupancies, we use the Methfessel-Paxton smearing method.[24] The adopted smearing width is 0.1 eV for the atomic relaxation and 0.02 for the accurate band structure analysis and density of states calculations. All structures have been treated within a supercell geometry using the periodic boundary conditions. The lattice constants of the tetragonal supercell in the x-y plane are taken as $a_{sc}=b_{sc}=25$ Å and $c_{sc}=c_o$ along the z axis. For the double unit cell calculations, the lattice constant is taken as $c_{sc}=2c_o$ to prevent the interactions between the nearest neighbor impurity atoms located in adjacent cells. In the self-consistent potential and total energy calculations, the Brillouin zone of SiNW is sampled in the **k** space within the Monkhorst-Pack scheme[25] by $(1\times1\times15)$ and $(1\times1\times11)$ mesh points for single and double cell, respectively. A plane wave basis set with kinetic energy in the range from 200 to 400 eV has been used depending on the impurity atom. All atomic positions and lattice parameters are optimized by using the conjugate gradient method where total energy and atomic forces are minimized. The convergence for energy is chosen as 10^{-5} eV between two ionic steps, and the maximum force allowed on each atom is 0.02 eV/Å.

III. BARE AND H SATURATED SiNW

In this study, we took a silicon nanowire as a prototype, which has $N=57$ Si atoms in its primitive unit cell and is grown along the [001] direction. The ideal nanowire is cut initially from bulk Si crystal and, subsequently, the lattice constant c_o and all the atomic positions are fully optimized. Upon relaxation, the structure of the ideal bare nanowire reconstructed. Furthermore, to allow possible reconstructions involving two unit cells, we carried out structure optimization of an ideal nanowire by doubling the primitive cell to include $N=114$ Si atoms. In the latter optimization, the energy per Si atom and the atomic structure did not change from the single cell optimization.The *ab initio* molecular dynamics calculations are carried out for SiNW at 500 K for 1 ps by rescaling velocities. The time step is taken as 3 fs. In order to allow reconstructions involving multiple unit cells, supercells involving two ($N=114$) and four ($N=228$) primitive unit cells have been used. These calculations indicate that SiNW is stable also at high temperature. The optimized structure is shown in Fig. 1. The average radius of the bare SiNW(57) is ~6.6 Å. In the case of H-SiNW(57), the dangling bonds on the surface of optimized bare SiNW are saturated with hydrogen atoms and the system is optimized again. From now on, structure optimized bare and hydrogen saturated silicon nanowires having $N=57$ silicon atoms in the primitive unit cell will be denoted as SiNW and H-SiNW, respectively. However, nanowire structures with periodicity involving double primitive unit cell with $N=114$ Si atoms will be specified as SiNW(114) or H-SiNW(114). It should be noted that the above sequence of structure optimization is in compliance with the fabrication of H-SiNW.[26] The average radius of the relaxed hydrogen saturated nanowire is found to be 8.9 Å. The lattice constants of optimized bare SiNW and H-SiNW are determined as 5.42 and 5.38 Å, respectively. These values are very close to the cubic lattice parameter of bulk crystal ($a=5.46$ Å) of Si. The Si-Si distance distributions of ideal SiNW, optimized bare SiNW, and optimized H-SiNW are shown in Fig. 1 up to the sixth nearest neighbor. Owing to reconstruction, the Si-Si distance distribution of the optimized bare SiNW deviates dramatically from that of the ideal SiNW. Upon passivation with H and subsequent optimization, most of the peak positions coincide with those of the ideal SiNW.

The cohesive energy is calculated as 4.24 eV, which is 0.40 eV less than that of the bulk Si crystal. While bare SiNW is metallic due to the dangling bonds on the surface, it becomes semiconductor with a direct band gap of 1.7 eV when the dangling bonds are saturated with H atoms. In view of the fact that GGA underestimates the band gaps, the system may have a wider direct band gap, which is very convenient for optoelectronic applications.[27] The total density of states (TDOS) and energy band diagrams are illustrated in

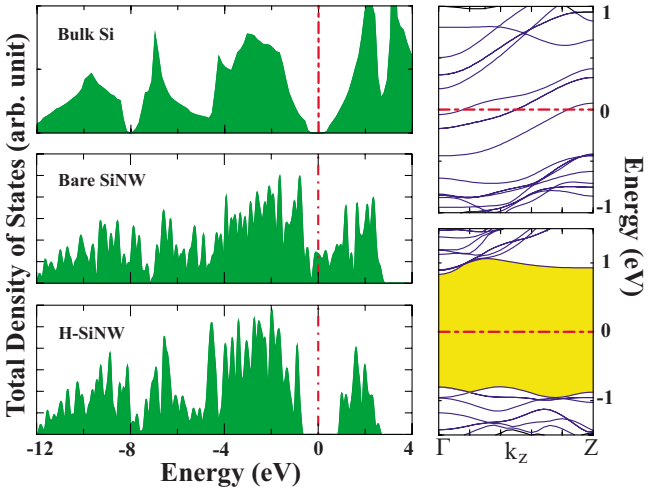

FIG. 2. (Color online) The left panels display the TDOS of bulk Si, optimized bare SiNW, and optimized H-SiNW. The right panels are the energy band diagrams for the optimized bare and hydrogenated silicon nanowires. The energy gap of semiconducting H-SiNW is shaded. The zero of energy is taken at the Fermi level.

Fig. 2. For the sake of comparison, TDOS of bulk Si is given on the left upmost panel.

IV. SINGLE ATOM ADSORPTION

A. Structure and energetics

Having discussed the structural and electronic properties of bare and H-SiNW, we now present a systematic analysis of the doping of various elements from group IIIA (Al, Ga), group IVA (C, Si, Ge), group VA (As, N, P), group VIA (Te) and also Pt as a TM element. In semiconductor physics, the doping normally indicates the minute concentration of foreign (impurity) atoms implemented substitutionally or interstitially into the crystal with an average nearest neighbor distance of several lattice parameters. An impurity state that cannot couple with the neighboring ones becomes localized (isolated) at the impurity site. The electron-electron interaction, the resulting dielectric constant ϵ_o, and the effective mass $m^\star$ of the band electrons determine the energy levels relative to the band edges and the effective radius of the donors or acceptors. However, the situation may be different for doped H-SiNWs because ϵ_o and $m^\star$ undergo a change due to size and dimensionality effects. Moreover, local environment, as well as coordination of an impurity in H-SiNW, can be different from its counterpart in bulk Si crystal. For example, an impurity can be adsorbed on the surface or substitute a Si atom either at the surface or in the core region. Here, we simulated the effect of doping by adsorbing a single impurity adatom to the surface either in every unit cell (having nearest neighbor distance $\ell_{n,n}=c_o$ and $N=57$) or in every two unit cells (having $\ell_{n,n}=2c_o$ and $N=114$). While the significant coupling in the case of high concentration leads to the formation of the bands, owing to the negligible coupling in the case of low concentration, the dopant adatom yields flat impurity bands. These flat bands may be taken to represent states of an isolated impurity. In order to find the energetically most favorable configuration of adatoms, we first consider six possible initial adsorption sites[28] on the surface of the nanowire, as described in Fig. 3. We initially place the adatom at one of these sites and fully relax the whole system in order to obtain the energetically most favorable configuration. In the relaxation process, structural deformations and also bond breaking of Si-Si or Si-H are allowed. The results that we have obtained from present calculations are summarized in Table I. The binding energy of elements are calculated from the following expression:

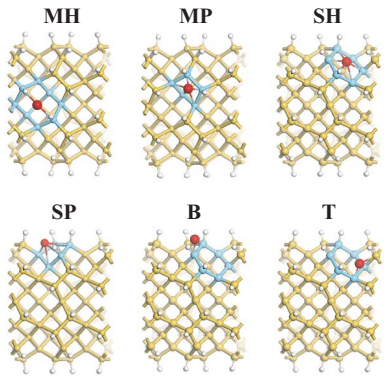

FIG. 3. (Color online) Possible adsorption sites of the adatom (impurity) at the surface. These sites are, respectively, the (1) hollow site of the surface hexagon at the concave part of the cross section (see Fig. 1) (*MH*), (2) hollow site of the surface pentagon at the concave part of the cross section (*MP*), (3) hollow site of the surface hexagon at the convex part of the cross section (*SH*), (4) hollow site of the surface pentagon at the convex part of the cross section (*SP*), (5) bridge site of hexagon at the convex part of the cross section (*B*), and (6) top sites (*T*).

$$E_b = E_T[\text{H-SiNW(N)}] + E_T[A] - E_T[\text{H-SiNW(N)} + A], \tag{1}$$

where $E_T[\text{H-SiNW(N)}+A]$ is the total energy of adatom A absorbed to H-SiNW(N), $E_T[\text{H-SiNW(N)}]$ is the total energy of H-SiNW(N), and $E_T[A]$ is either the spin-polarized or spin-unpolarized energy of the adsorbed atom calculated within the same supercell.[29] In the case of single unit cell calculations with $N=57$, the distance between adatoms is $\ell_{n,n}=5.38$ Å so that the interaction may not be negligible. For double cell calculations, $c_{sc}=\ell_{n,n}=10.76$ Å and $N=114$. For all the elements under consideration, E_b is considerably high, which indicates a chemical interaction between adatom and H-SiNW.

We found that the energetically most favorable adsorption site depends on the group of the Periodic Table that the adatom belongs to. For example, site *MH* is found to be favored by the group IIIA elements (namely, Al, Ga). On the other hand, elements of groups IVA, VA, and VIA prefer site *B*. Platinum, being a TM element, prefers site *SH* after atomic relaxation. First row elements, C and N, having the smallest radius among all elements studied here, are adsorbed with a high binding energy $E_b=8.06$ and 8.71 eV, respectively. These two atoms first break Si–Si bond to form Si–A–Si bond and also attract the H atom of the neighboring Si–H

TABLE I. Initial positions of the impurities (adatoms) are indicated with abbreviations such as *MH*, *MP*, *SH*, *SP*, *B*, and *T*, as described in Fig. 3. Single cell (double cell) signifies that the periodic nearest neighbor distance of the adatoms is $\ell_{n,n}=c_o$ ($\ell_{n,n}=2c_o$). Final optimized configurations are denoted, for example, as $\rightarrow MH$. Superscript *b* means that adatom breaks Si-Si bond(s) in the vicinity of its initial position. Subscript *h* indicates breaking and binding of hydrogen atom by the adatom. E_b^{up} (E_b^{sp}) and E_b^b correspond to the impurity binding energy relative to spin-unpolarized (spin-polarized) free atom and bulk energies of impurity atom, respectively. *d* shows the distance between adatom and nearest neighbor Si atoms.

		MH	*MP*	*SH*	*SP*	*B*	*T*	Double cell
Al		$\rightarrow MH$	$\rightarrow MH$	$\rightarrow B$	$\rightarrow B$	$\rightarrow B$	$\rightarrow MH$	$\rightarrow MH$
	E_b^{up} (eV)	1.64	1.65	1.33	1.31	0.88	1.60	1.69
	E_b^{sp} (eV)	1.57	1.58	1.26	1.24	0.81	1.53	1.51
	E_b^b (eV)	−1.75	−1.75	−2.07	−2.09	−2.52	−1.79	−1.95
	d (Å)	2.86	2.86	2.79	2.84	2.83	2.86	2.84
Ga		$\rightarrow MH$	$\rightarrow MH$	$\rightarrow SP$	$\rightarrow SP$	$\rightarrow B$	$\rightarrow MH$	$\rightarrow MH$
	E_b^{up} (eV)	1.36	1.36	1.14	1.14	0.78	1.35	1.43
	E_b^{sp} (eV)	1.28	1.28	1.08	1.07	0.71	1.28	1.26
	E_b^b (eV)	−1.29	−1.29	−1.50	−1.50	−1.86	−1.29	−1.51
	d (Å)	2.84	2.84	2.90	2.92	2.85	2.91	2.90
C		$\rightarrow B^b$	$\rightarrow B^b$	$\rightarrow SH^b$	$\rightarrow SP^b$	$\rightarrow B_h^b$	$\rightarrow T^b$	$\rightarrow B_h^b$
	E_b^{up} (eV)	6.64	6.88	6.14	7.04	8.06	6.54	8.35
	E_b^{sp} (eV)	5.22	5.46	4.72	5.62	6.64	5.11	8.35
	E_b^b (eV)	−2.42	−2.18	−2.91	−2.02	−1.0	−2.52	−0.71
	d (Å)	1.80	1.86	1.91	1.92	1.78	1.81	1.78
Si		$\rightarrow MH$	$\rightarrow MH$	$\rightarrow SH^b$	$\rightarrow SP^b$	$\rightarrow B_h$	$\rightarrow T_h$	$\rightarrow B_h$
	E_b^{up} (eV)	2.53	2.53	2.60	2.37	3.33	3.20	3.54
	E_b^{sp} (eV)	1.90	1.90	1.97	1.74	2.70	2.58	2.79
	E_b^b (eV)	−2.65	−2.65	−2.58	−2.81	−1.85	−1.97	−1.84
	d (Å)	2.54	2.54	2.44	2.56	2.51	2.49	2.51
Ge		$\rightarrow MH$	$\rightarrow MH$	$\rightarrow B$	$\rightarrow SP^b$	$\rightarrow B_h$	$\rightarrow T_h$	$\rightarrow B_h$
	E_b^{up} (eV)	2.10	2.10	1.97	2.03	2.69	2.61	2.94
	E_b^{sp} (eV)	1.54	1.54	1.41	1.47	2.13	2.04	2.26
	E_b^b (eV)	−2.15	−2.15	−2.27	−2.21	−1.56	−1.64	−1.53
	d (Å)	2.72	2.68	2.58	2.59	2.44	2.40	2.45
N		$\rightarrow B^b$	$\rightarrow B^b$	$\rightarrow B^b$	$\rightarrow B^b$	$\rightarrow B_h^b$	$\rightarrow T^b$	$\rightarrow B_h^b$
	E_b^{up} (eV)	8.34	7.63	8.50	7.54	8.71	7.61	8.99
	E_b^{sp} (eV)	5.13	4.42	5.29	4.33	5.50	4.40	5.78
	E_b^b (eV)	3.6	2.89	3.76	2.80	3.97	2.87	4.24
	d (Å)	1.78	1.80	1.77	1.80	1.74	1.79	1.75
P		$\rightarrow B^b$	$\rightarrow MP^b$	$\rightarrow B^b$	$\rightarrow SP^b$	$\rightarrow B_h^b$	$\rightarrow T_h$	$\rightarrow B^b$
	E_b^{up} (eV)	4.47	3.46	4.48	3.31	4.40	3.88	4.52
	E_b^{sp} (eV)	2.80	1.78	2.80	1.64	2.72	2.21	2.76
	E_b^b (eV)	−0.72	−1.73	−0.71	−1.88	−0.79	−1.31	−0.77
	d (Å)	2.27	2.27	2.28	2.27	2.27	2.36	2.21
As		$\rightarrow B^b$	$\rightarrow B^b$	$\rightarrow B^b$	$\rightarrow B^b$	$\rightarrow B_h^b$	$\rightarrow T_h$	$\rightarrow B^b$
	E_b^{up} (eV)	3.63	3.63	3.64	3.60	3.43	3.11	3.85
	E_b^{sp} (eV)	2.19	2.19	2.20	2.16	1.99	1.68	2.29
	E_b^b (eV)	−0.86	−0.86	−0.85	−0.89	−1.06	−1.38	−0.77
	d (Å)	2.41	2.41	2.42	2.42	2.40	2.36	2.33

TABLE I. (*Continued.*)

		MH	*MP*	*SH*	*SP*	*B*	*T*	Double cell
Te		$\rightarrow B^b$	$\rightarrow MP^b$	$\rightarrow T_h$	$\rightarrow B^b$	$\rightarrow T_h$	$\rightarrow T_h$	$\rightarrow B^b$
	E_b^{up} (eV)	2.94	2.08	2.78	2.02	2.73	2.74	2.86
	E_b^{sp} (eV)	2.42	1.56	2.26	1.50	2.20	2.22	2.29
	E_b^b (eV)	0.019	−0.85	−0.14	−0.91	−0.20	−0.19	−0.20
	d (Å)	2.52	2.69	2.54	2.51	2.53	2.54	2.52
Pt		$\rightarrow MH$	$\rightarrow MP^b$	$\rightarrow SH$	$\rightarrow SP^b$	$\rightarrow B_h$	$\rightarrow T$	$\rightarrow SH$
	E_b^{up} (eV)	5.24	5.03	5.49	5.07	4.38	4.72	5.63
	E_b^{sp} (eV)	4.99	4.79	5.24	4.82	4.14	4.47	5.30
	E_b^b (eV)	−0.53	−0.74	−0.28	−0.70	−1.38	−1.05	−0.24
	d (Å)	2.42	2.39	2.48	2.40	2.38	2.38	2.48

bond to form A–H bond (i.e., C–H or N–H) specified as B_h^b configuration in Table I. Si and Ge adatoms are adsorbed at the bridge position above the Si-Si bond without any significant deformation at the underlying Si nanowire but break the Si–H bond and bind the freed H atom. This adsorption configuration is specified as B_h. P, As, and Te are adsorbed at site B^b, but they cannot break the neighboring Si–H bond. Pt has also high binding energy (5.24 eV). Unlike the other elements, Pt has moved inward after relaxation. Besides, Pt–Si bond length is measured as 2.5 Å, which is comparable to the Pt–Pt bond distance (2.8 Å) in bulk Pt. The binding energies with respect to the element's bulk cohesive energy are always negative except for N. This means that nitrogen doping is an exothermic process in which energy is given out from the system. Note that N is the only element studied in this work, being in the gaseous state at room temperature, while others are in solid state. Interestingly, there exists a trend in binding energies of elements within the same group in such a way that it decreases as the radius of the element increases. While the distance of Al and Ga to the nearest Si atoms is $d=2.9$ Å, this distance ranges between 2.3 and 2.5 Å for other elements except C and N. Carbon and nitrogen, having the smallest radius among other impurities, have the smallest distance to the nearest neighbor Si atoms.

In the double cell calculations ($\ell_{n,n}=2c_o$), we considered only the most energetic sites determined in single cell calculations. By placing the adatom to the same position in every two cells, we relaxed the whole system to minimize the total energy. Results are given in the last column of Table I. After the atomic relaxation, we observed similar effects, such as breaking of Si–Si and Si–H bonds and also binding of H by the same adatoms discussed in single cell calculations. The trend in binding energy of adatom which decreases as it moves down within the same group elements is also observed in double cell calculations. Furthermore, the binding energies which are calculated by using Eq. (1) in double cell slightly increase as compared to the single cell results. As ℓ_{nn} increases from 5.38 to 10.76 Å, the interaction between adatoms reduces, whereby adatom-wire interaction is enhanced. E_b, with respect to bulk cohesive energies, remains negative except for nitrogen again. The nearest adatom-Si distance, d does not significantly change from single cell values.

Finally, we note that binding energies in Table I corresponding to the same final optimized adsorption geometry which initiates from different adsorption sites may differ slightly. This is due to the different paths of the impurity atom between the final and different initial configurations, whereby the final geometry may deviate slightly from the minimum total energy configuration. Here, the highest value of E_b has to be taken as the binding energy of the final, most energetic adsorption site. However, there are significant energy differences between the same B (or B^b) optimized final adsorption geometry. This originates from the bridge sites of the hexagonal or pentagonal rings.

B. Electronic properties

We first consider adatom adsorption at high concentration with $\ell_{n,n}=c_o$, where the electronic structure of H-SiNW is affected considerably. The energy band diagrams are illustrated in Fig. 4. Semiconducting H-SiNW becomes metallic upon adsorption of IIIA and VA elements, which have an odd number of valence electrons. For these systems, one nondegenerate half-filled band crosses the Fermi energy E_F. According to the band decomposed charge density analysis, these bands originate from the impurity atom. The dispersion of these bands indicate a non-negligible coupling between adatoms. The quantum ballistic conductance[30] of such an infinite metallic wire at small bias is $G=2e^2/h$. The conductance of the finite wire is, however, smaller than $2e^2/h$ due to connections to the electrode. For the other elements which have an even number of valence electrons, the wire remains semiconducting with modified band gaps. C and Pt doped H-SiNWs have again a direct band gap of 1.17 and 1.36 eV, respectively, whereas Ge, Si, and Te atoms change H-SiNW from the direct band gap to the indirect band gap of 1.46, 1.41, and 1.54 eV, respectively.[31] Commonly, we observe that the band gap value decreases after the adsorption of the adatom.

Next, we examine the electronic structure at low concentration of the adatom obtained from double cell calculations with $\ell_{n,n}=2c_o$. The corresponding energy band structures are presented in Fig. 5. Due to the reduced interaction between adatoms, the dispersion of the bands near E_F is low. These

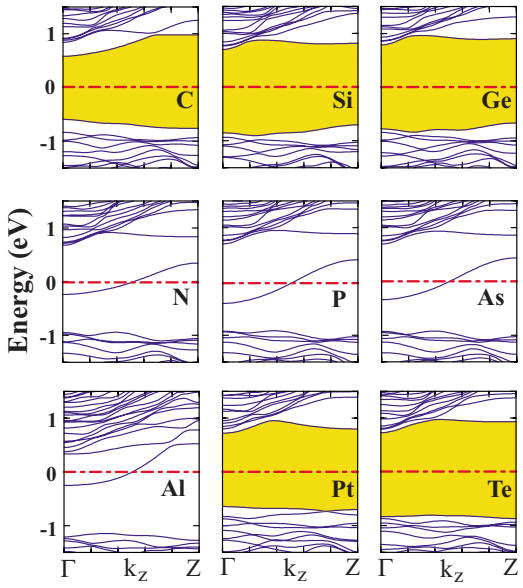

FIG. 4. (Color online) Energy band structures of adatom (impurity) adsorbed H-SiNW. The distance between adjacent impurity atoms is $\ell_{n,n}=c_o=5.38$ Å. The energy gaps of semiconducting structures are highlighted. The dash-dotted line represents the Fermi level. Note that owing to the significant adatom-adatom interaction, the width of the impurity bands is in the range of 0.5–1 eV.

bands may be assumed to correspond to the isolated impurity levels. At very low concentration (which cannot be treated by the present method), the isolated impurity levels do not coincide with the Fermi level.[32] Interestingly, while the impurity level that coincides with the Fermi energy is closer to the valence band for the case of P and As doped H-SiNW(114), it lies at the middle of the band gap of the N doped nanowire. Surprisingly, Al doping causes energy levels to shift closer to the conduction band. The location of impurity states in the band gap occurs in a reverse order as compared to the *n*-type (N, P, As) and *p*-type (Al, Ga) dopants in bulk Si crystal. In fact, Singh *et al.*[10] have studied the effects of substitutional P impurity on the electronic and atomic structures of H-SiNW (along the [110] direction and having a square cross section) using a similar *ab initio* method. The Fermi level was seen to shift toward the conduction band while making the nanowire *n* type. This situation is explained by the fact that in the present case, the adatoms are simply absorbed on the surface of H-SiNW. Similar to the single cell analysis, C and Te doped H-SiNW(114) have again direct and indirect band gaps, respectively. On the other hand other elements change the nanowire from the direct band gap into the indirect band gap or vice versa. Besides, the energy gap values are increased as compared with the single cell results. Although *n*- or *p*-type impurity effects cannot be observed in the case of adsorbed adatom type, one can tune the band gap of the doped nanowire easily. This is a promising result for optoelectronic applications. However, it should be noted that the effect of impurity on the band gap diminishes as the concentration of adatom decreases and, hence, $\ell_{n,n}$ becomes several c_o. The band decomposed charge density analysis clearly indicates the character of the impurity level. These bands belong to *p* orbitals of dopant atoms.

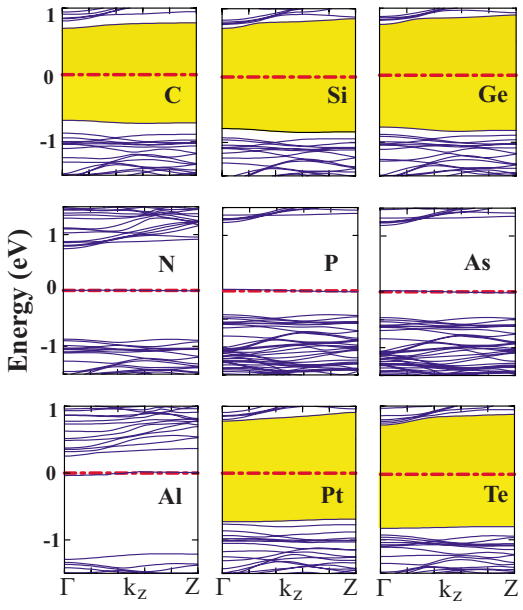

FIG. 5. (Color online) Energy band structures of adatom (impurity) adsorbed H-SiNW(114) with $\ell_{n,n}=2c_o=10.76$ Å. The energy gaps of semiconducting structures are again highlighted. The flat bands which line up with the Fermi energy are reminiscent of isolated impurity levels.

V. SUBSTITUTION

In addition to adatom adsorption on the surface of SiNW, substitutional impurities such as Al and As have also been examined. To this end, one Si atom in the core or on the surface of H-SiNW(114) was replaced with either Al or As atom. The substitution energy is calculated as follows:

$$E_s = E_T[\text{H-SiNW}(114)] + E_T[S] - E_T[\text{H-SiNW}(113)+S] - E_T[\text{Si}], \quad (2)$$

where S denotes the free impurity atom, and $E_T[\text{H-SiNW}(113)+S]$ is the total energy of the optimized system where one Si atom is replaced by S. After the full relaxation of the system, surface configurations were seen to be more favorable when compared with the core ones, in agreement with earlier calculations dealing with B and P doped Si nanowires.[10,11] The substitution energies of dopants relative to the spin-unpolarized (spin-polarized) dopant free atom energy and their bulk energies are given in Table II. The energy band diagrams are presented in Figs. 6 and 7 together with their charge analysis. As one can see, it is possible to make *p*-type (*n*-type) silicon nanowire by doping with Al (As) atom substitutionally. The isosurface charge analysis presented in Fig. 6 displays *p*-type orbital characteristics for the levels crossing the Fermi energy. The nondegenerate band with negligible dispersion originates mainly from Al orbitals and is reminiscent of the acceptor state at very low Al concentration. On the other hand, a hybridized state which is composed of As and its nearest neighbor Si atoms is obtained for the As doped nanowire. Flat As impu-

TABLE II. Substitution energy of the substitutional impurities (Al and As). E_s^{up}, E_s^{sp}, and E_s^b are defined as in the caption of Table I and Eq. (2).

	E_s^{up} (eV)	E_s^{sp} (eV)	E_s^b (eV)		E_s^{up} (eV)	E_s^{sp} (eV)	E_s^b (eV)
$Al_{surface}$	−2.72	−2.15	−0.97	$As_{surface}$	−1.40	−2.22	−0.65
Al_{core}	−3.00	−2.44	−1.26	As_{core}	−1.53	−2.35	−0.78

rity bands occur near the conduction band edge, attributing an *n*-type character to the dopant. At very low As concentration, these flat bands become isolated donor states near the conduction band edge. For the case of surface substitutional doping, the isosurface charge analysis of those nondegenerate single levels crossing the Fermi energy are again purely *p*-type dopant states. We note, however, that energies relative to the band edges and characters of these donor and acceptor states are closely related to the configuration of the corresponding substitutional impurity.

VI. DISCUSSION AND CONCLUSIONS

In this paper, we presented a systematic study of the effect of doping of silicon nanowire by several impurity atoms. We took a hydrogenated Si nanowire as prototype and investigated the adsorption and substitution onto the surface, as well as the substitution of impurity atom in the core. The adsorption of impurity atom on the surface has been treated in the high concentration (one adatom per unit cell of 57 Si atoms) and "low" concentration (one adatom per two unit cells of 114 Si atoms) limits. The usual band theory yields impurity bands for both concentration limits, the high concentration bands being dispersive and the low concentration bands being flat. The latter flat bands have been taken as representative of single impurity levels. Our analysis reveals that SiNW surface impurity sites are very active and strongly interacts with IIIA, IVA, VA, and VIA elements. While IIIA elements (Al, Ga) prefer to be at the center of the middle hexagon and do not distort the SiNW surface, the elements in other groups break the Si–Si bond(s) of the nanowire. C and N even break Si–H bond and bind the hydrogen atom to themselves. Different from the elements in groups IIIA, IVA, VA, and VIA, Pt prefers the hollow site of the hexagon being in the same plane as Si atoms. Initially semiconducting H-SiNW becomes metallic when IIIA and VA elements are

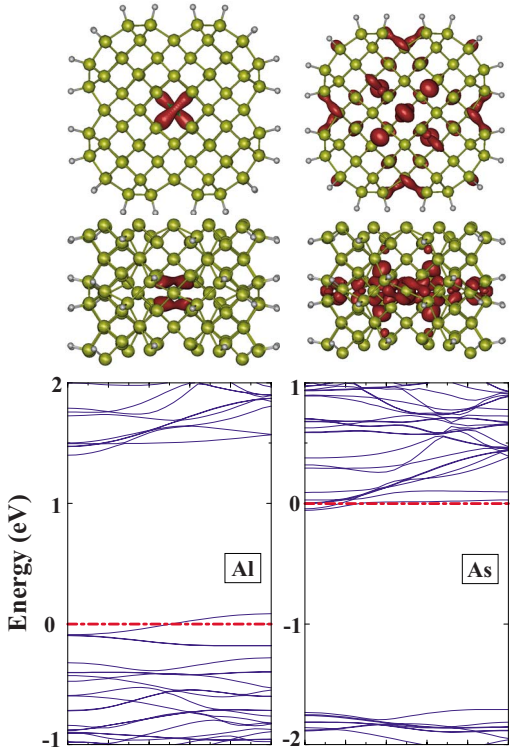

FIG. 6. (Color online) Si atom in the core of H-SiNW(114) is replaced with impurity atom (Al or As). On the left, Al replaced one of the core Si atoms. The charge density graph is given at the top, indicating *p*-orbital characteristics. The energy band structure at the bottom indicates a *p*-type behavior. On the right, the charge density graph and energy band structure of As replacing one of the core Si atoms are presented. All these analyses are realized for the double unit cell.

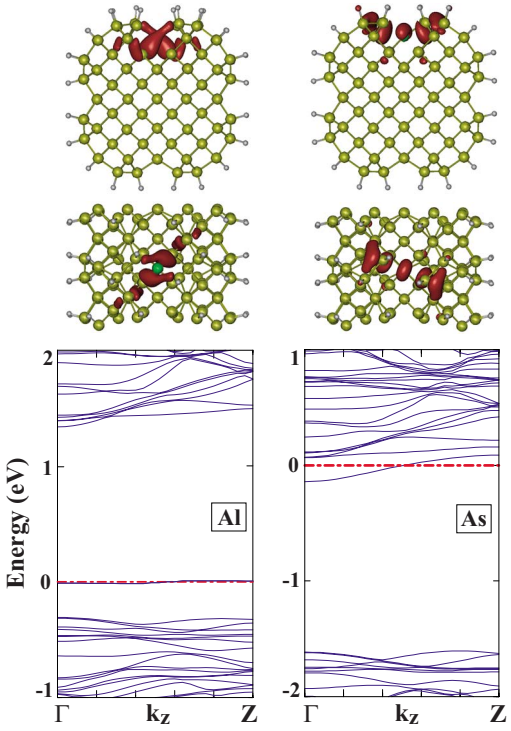

FIG. 7. (Color online) Si atom on the surface of H-SiNW(114) is replaced with either Al or As atom. *p*-orbital characteristics of impurity states and *p*-type (Al) and *n*-type (As) behaviors of semiconducting are clearly seen.

adsorbed in the high concentration limit. However, it remains semiconducting with a modified band gap when doped with other elements that have even number of valence electrons. Similar trends are also obtained in the low concentration limit. Due to the reduced adatom-adatom interaction, dispersionless impurity bands are obtained. The band decomposed charge density analysis indicates that these levels originate from doping elements. H-SiNW semiconductor can be modified as a *p* type and an *n* type through substitution of Al and As, respectively. In view of the above results, one can contemplate that metallic, *n* and *p*-type zones or any sequence and size of them can be generated according to a desired device functionality. This way, various types of devices and a metallic interconnect between them can be realized using the same Si nanowire. In particular, metal-semiconductor junctions shall easily be produced. It is expected that the above trends exist in other H-SiNWs with $N>57$. In conclusion, our results indicate that the electronic properties of SiNW can be modified by single atom adsorption according to the desired properties and can be used in nanoscale device applications.

ACKNOWLEDGMENT

Part of the computations has been performed using the ULAKBİM High Performance Computer Center.

*ciraci@fen.bilkent.edu.tr

[1] Y. Cui, Z. Zhong, D. Wang, W. U. Wang, and C. M. Lieber, Nano Lett. **3**, 149 (2003).
[2] Y. Huang, X. F. Duan, and C. M. Lieber, Small **1**, 142 (2005).
[3] X. F. Duan, Y. Huang, R. Agarwal, and C. M. Lieber, Nature (London) **421**, 241 (2003).
[4] D. D. D. Ma, C. S. Lee, F. C. K. Au, S. Y. Tong, and S. T. Lee, Science **299**, 1874 (2003).
[5] R. Rurali and N. Lorente, Phys. Rev. Lett. **94**, 026805 (2005).
[6] A. K. Singh, V. Kumar, R. Note, and Y. Kawazoe, Nano Lett. **5**, 2302 (2005).
[7] Y. Zhao and B. Yakobson, Phys. Rev. Lett. **91**, 035501 (2003); S. Ismail-Beigi and T. Arias, Phys. Rev. B **57**, 11923 (1998).
[8] R. Q. Zhang, Y. Lifshitz, D. D. D. Ma, Y. L. Zhao, Th. Frauenheim, S. T. Lee, and S. Y. Tong, J. Chem. Phys. **123**, 144703 (2005).
[9] P. W. Leu, B. Shan, and K. Cho, Phys. Rev. B **73**, 195320 (2006).
[10] A. K. Singh, V. Kumar, R. Note, and Y. Kawazoe, Nano Lett. **6**, 920 (2006).
[11] M. V. Fernandez-Serra, Ch. Adessi, and X. Blase, Phys. Rev. Lett. **96**, 166805 (2006).
[12] Y. Cui, Q. Q. Wei, H. K. Park, and C. M. Lieber, Science **293**, 1289 (2001).
[13] X. T. Zhou, J. Q. Hu, C. P. Li, D. D. D. Ma, C. S. Lee, and S. T. Lee, Chem. Phys. Lett. **369**, 220 (2003).
[14] J. Hahm and C. M. Lieber, Nano Lett. **4**, 51 (2004).
[15] E. Durgun, D. Cakir, N. Akman, and S. Ciraci, arXiv:0704.0109.
[16] H. Sellier, G. P. Lansbergen, J. Caro, S. Rogge, N. Collaert, I. Ferain, M. Jurczak, and S. Biesemans, Phys. Rev. Lett. **97**, 206805 (2006).
[17] S. Sirichantaropass, V. M. Garcia-Suarez, and C. J. Lambert, e-print arXiv:cond-mat/0611128.
[18] M. C. Payne, M. P. Teter, D. C. Allen, T. A. Arias, and J. D. Joannopoulos, Rev. Mod. Phys. **64**, 1045 (1992).
[19] Numerical computations have been carried out using VASP software. G. Kresse and J. Hafner, Phys. Rev. B **47**, R558 (1993); G. Kresse and J. Furthmuller, *ibid.* **54**, 11169 (1996).
[20] W. Kohn and L. J. Sham, Phys. Rev. **140**, A1133 (1965); P. Hohenberg and W. Kohn, Phys. Rev. **136**, B864 (1964).
[21] D. Vanderbilt, Phys. Rev. B **41**, R7892 (1990).
[22] We used the following configurations for the atomic pseudopotentials: Al and Ga: s^2p^1; C, Si, and Ge: s^2p^2; N, P, and As: s^2p^3; Te: s^2p^4; Pt: s^1d^9.
[23] J. P. Perdew, J. A. Chevary, S. H. Vosko, K. A. Jackson, M. R. Pederson, D. J. Singh, and C. Fiolhais, Phys. Rev. B **46**, 6671 (1992).
[24] M. Methfessel and A. T. Paxton, Phys. Rev. B **40**, 3616 (1989).
[25] H. J. Monkhorst and J. D. Pack, Phys. Rev. B **13**, 5188 (1976).
[26] In the present study, H-SiNW is obtained in following sequences: First, the ideal SiNW is cut from the ideal, tetrahedrally coordinated bulk Si crystal. Ideal and bare SiNW is then fully optimized. The structure of this bare nanowire is shown in Fig. 1. This optimized bare SiNW is passivated with H atoms and eventually optimized again. Note that this sequence leads to electronic properties different from the sequence where the ideal bare SiNW is passivated and then optimized.
[27] According to the GW corrections carried out by X. Zhao, C. M. Wei, L. Yang, and M. Y. Chou, Phys. Rev. Lett. **92**, 236805 (2004), the actual band gap of H-SiNW(57) is estimated to be $\sim$2.3 eV.
[28] There are other sites on the surface for the adsorption of atoms that are left out of the scope of the present study. For example, in addition to the bridge sites of surface hexagons (*BH*), there are two types of bridge sites of surface pentagons, namely, one between the two adjacent pentagons and the other one between the adjacent hexagon and pentagon. Our test calculations showed that these two sites are not stable sites for adatom.
[29] In this way, the adatom-adatom coupling is excluded in the value of binding energy E_b.
[30] Note that such a half-filled metallic band is vulnerable to the Peierls distortion.
[31] In these band gap values, the GW self-energy corrections are not taken into account.
[32] Statistical calculations based on the law of mass action [see, for example, C. Kittel, *Introduction to Solid State Physics*, 7th ed. (Wiley, New York, 1996)] at low concentration and finite temperature indicate that the chemical potential shifts from the isolated impurity levels.